Alternative Splicing of a β_4 Subunit Proline-Rich Motif Regulates Voltage-Dependent Gating and Toxin Block of $Ca_v2.1$ Ca^{2+} Channels

Thomas D. Helton,[1] Douglas J. Kojetin,[2] John Cavanagh,[2] and William A. Horne[1]

Departments of [1]Molecular Biomedical Sciences and [2]Molecular and Structural Biochemistry, North Carolina State University, Raleigh, North Carolina 27606

Ca^{2+} channel β subunits modify α_1 subunit gating properties through direct interactions with intracellular linker domains. In a previous report (Helton and Horne, 2002), we showed that alternative splicing of the β_4 subunit had α_1 subunit subtype-specific effects on Ca^{2+} channel activation and fast inactivation. We extend these findings in the present report to include effects on slow inactivation and block by the peptide toxin ω-conotoxin (CTx)-MVIIC. N-terminal deletion and site-directed mutagenesis experiments revealed that the effects of alternative splicing on toxin block and all aspects of gating could be attributed to a proline-rich motif found within N-terminal β_{4b} amino acids 10–20. Interestingly, this motif is conserved within the third postsynaptic density-95 (PSD-95)/Discs large/zona occludens-1 domain of the distantly related membrane-associated guanylate kinase homolog, PSD-95. Sequence identity of ~30% made possible the building of β_{4a} and β_{4b} three-dimensional structural models using PSD-95 as the target sequence. The models (1) reveal that alternative splicing of the β_4 N terminus results in dramatic differences in surface charge distribution and (2) localize the proline-rich motif of β_{4b} to an extended arm structure that flanks what would be the equivalent of a highly modified PSD-95 carboxylate binding loop. Northern blot analysis revealed a markedly different pattern of distribution for β_{4a} versus β_{4b} in the human CNS. Whereas β_{4a} is distributed throughout evolutionarily older regions of the CNS, β_{4b} is concentrated heavily in the forebrain. These results raise interesting questions about the functional role that alternative splicing of the β_4 subunit has played in the evolution of complex neural networks.

Key words: calcium channel; β_4 subunit; PSD-95; alternative splicing; gating; N terminus; ω-CTx-MVIIC

Voltage-gated Ca^{2+} channels participate in an extensive array of cellular activities including excitation–contraction coupling, transcription, and neurotransmitter release. Neuronal Ca_v2 channels are assemblies of up to five subunits, α_1, α_2/δ, β, and γ. The α_1 subunit consists of four homologous repeats (I–IV) of six helices (S1–S6) that arrange to form the selectivity filter and pore. The 24 transmembrane helices are connected by a series of alternating intracellular and extracellular loops. These loops are targets for a host of modifying proteins, including β subunits, G-proteins, calmodulin, and syntaxin, as well as the peptide toxins of venomous spiders and marine snails (Catterall, 2000). Interaction of these proteins with α_1 subunits typically alters the voltage dependency and kinetics of channel gating, which in turn modifies Ca^{2+} entry into neurons.

Ultimately, gating behavior is determined by the interactions of individual amino acid side chains with the electrostatic forces within their microenvironments. This is especially true for the positively charged S4 helical segments that constitute the voltage sensors in Na^+, Ca^{2+}, and K^+ channels. Biophysical studies have shown that depolarization disrupts S4 side-chain interactions of Shaker K^+ channels to the extent that S4 helices rotate 180° along their axes (Cha et al., 1999; Glauner et al., 1999). This motion likely triggers a cascade of side-chain disruptions that ultimately leads to rotation and separation of the intracellular S6 segments that form the K^+ channel gate (Bezanilla, 2000). Such a mechanism is supported by recent studies delineating the conformational changes associated with open and closed states of bacterial two-membrane-spanning K^+ channels (Jiang et al., 2002b) and is generally applicable to Na^+ and Ca^{2+} channel gating.

Attempts have been made to assign specific gating functions to individual Ca^{2+} channel homology domains. Early chimera studies indicated that the IS6 segment was critical for setting the rate of fast inactivation (Zhang et al., 1994); however, substitution of IIS6 and IIIS6 of the $Ca_v2.3$ channel into the slow inactivating $Ca_v1.2$ channel caused a leftward shift in the voltage dependence of inactivation and increased the rate of $Ca_v1.2$ channel inactivation to near $Ca_v2.3$ rates (Stotz et al., 2000). Effects on gating have been reported for amino acid substitutions in IS3 (Zhong et al., 2001), the I-II linker (Berrou et al., 2001), IIS6 (Stotz and Zamponi, 2001), extracellular linkers IIIS3-S4 (Lin et al., 1997), and IVS3-S4 (Hans et al., 1999), and IVS6 (Berjukow et al., 2001). Additive effects on $Ca_v1.2$ channel inactivation were reported recently for individual IS6, IIS6, IIIS6, and IVS6 substitutions (Shi and Soldatov, 2002). Together, these data support a structural model of α_1 subunits in which individual transmembrane segments are interdependently entwined (Horn, 2000).

Our results indicate that this model also applies to β subunit interactions with α_1 subunit intracellular linkers. We have shown previously that β_4 subunit alternative splicing had α_1 subtype-

Received July 10, 2002; revised Aug. 22, 2002; accepted Aug. 22, 2002.

This work was supported by National Institutes of Health Grants NS32094 (W.A.H.) and GM5576 (J.C.), by a College of Veterinary Medicine State Research Support grant (W.A.H.), and by an award from the North Carolina State University Keenan Institute (J.C.).

Correspondence should be addressed to William A. Horne, Department of Molecular Biomedical Sciences, North Carolina State University, College of Veterinary Medicine, 4700 Hillsborough Street, Raleigh, NC 27606. E-mail: bill_horne@ncsu.edu.

specific effects on voltage-dependent activation and inactivation (Helton and Horne, 2002). In this report, we extend these findings to include effects on slow inactivation and block by ω-conotoxin (CTx)-MVIIC; we also identify a proline-rich motif in β_{4b} that is responsible for the observed differences in effects.

MATERIALS AND METHODS

Deletion mutants. Truncation of the β_{4b} N terminus in 10 aa increments was performed using PCR and custom oligonucleotide primers [Integrated DNA Technologies (IDT), Coralville, IA]. All nucleotide and amino acid positions for primers and restriction enzymes correspond to the β_{4b} sequence (GenBank accession number U95020). Each forward primer sequence contained an idealized Kozak (1991) sequence and start codon corresponding to the beginning of each of the deleted 10 amino acids as follows: β_{4b} Δ1–10F, 5′-GCCACCATGACCGCGGACGGGCCG; β_{4b} Δ1–20F, 5′-GCCACCATGCAGGTGGCCCGAGGC. Both reactions included a common β_4 reverse primer, β_{4b} 732R (5′-TGACGGCCCCACTAACACC). Full-length β_{4b} was used as the template for these reactions. The β_{4b} Δ10–20 deletion mutant was generated with the primer β_{4b} Δ10–20F (5′-GCCACCATGTCCTCCTCCTCCTACGCCAAGAACTCG) paired with β_{4b} 732R using the β_{4b} Δ1–20 mutant as the template. Annealing temperature for PCR was 56°C with Gene Choice *Taq* DNA polymerase (PGC Scientific, Durham, NC). Correctly sized PCR fragments were cloned into the pT-Advantage vector (Clontech, Palo Alto, CA). PCR-based cycle sequencing (FS chemistry; Applied Biosystems, Foster City, CA) was used with an ABI Prism 310 Genetic Analyzer. The data were analyzed using ABI Prism DNA sequencing software (version 2.12; PerkinElmer Biosystems), and sequence alignments and restriction maps were generated using Lasergene Software (DNA Star, Madison, WI). Correct clones were digested with *Bam*HI (Roche Molecular Biochemicals, Indianapolis, IN), and the corresponding ~530 bp fragments were ligated into *Bam*HI (nucleotide position 550) -digested β_{4b} in pBluescript II S/K$^+$ (Stratagene, La Jolla, CA). Each β_{4b} deletion mutant was sequenced to confirm correct reading frame and proper N-terminal orientation.

Site-directed mutagenesis. For all β_{4b} site-directed mutants, full-length β_{4b} cDNA (U95020) was used as the template unless otherwise indicated. All site-directed mutagenesis reactions were performed using a QuikChange site-directed mutagenesis kit (Stratagene) and custom forward and reverse compliment oligonucleotide primers (IDT): β_{4b}G10A,D13A, 5′-ACGCCAAGAACGCGACCGCGGCCGGGCCGCAC; β_{4b}P15A,P18A, 5′-GCGGACGGGGCGCACTCCGCCACCTCGCAGGTG; β_{4b}G10A,D13A,P15A,P18A, 5′-ACGCCAAGAACGCGACCGCGGCCGGGGCGCAC (β_{4b}P15A,P18A used as template); β_{4b}G10A,P15A, 5′-TACGCCAAGAACGCGACCGCGGACGGGGCGCACTCCCCCACCTCGCAGGTG; β_{4b}H16A, 5′-ACCGCGGACGGGCCGGCCTCCCCCACCTC; β_{4b}G10A,P18A, 5′-TACGCCAAGAACGCGACCGCGGACGGGCCGCACTCCGCCACCTCGCAGGTG;β_{4b}D13A,P15A, 5′-TACGCCAAGAACGGGACCGCGGCCGGGGCGCACTCCCCCACCTCGCAGGTG; β_{4b}D13A,P18A, 5′-TACGCCAAGAACGGGACCGCGGCCGGGCCGCACTCCGCCACCTCGCAGGTG;β_{4b}H16A, 5′-ACCGCGGACGGGCCGGCCTCCCCCACCCTCG; and β_{4b}T11A,S17A,T19A, S20A, 5′-CAAGAACGGGGCCGCGGACGGGCCGCACGCCCCCGCCGCGCAGGTGGCC. Each of the mutant clones was sequenced to confirm reaction fidelity.

Electrophysiology. cRNAs were synthesized *in vitro* using an mMessage mMachine RNA transcription kit from Ambion (Austin, TX) (T3 or T7 depending on clone orientation in pBluescript II S/K$^+$). Standard *Xenopus laevis* oocyte expression methods were used to characterize β deletion and site-directed mutants. Briefly, full-length α_1, α_2/δ-1, and β_4 cRNAs were injected in equimolar ratios (5.6 ng of α_{1A}, 2.4 ng of α_2/δ-1, and 1.6 ng of β_4 in 46 nl) into defolliculated oocytes (stage V–VI). The BI-2 (α_{1A}) and α_2/δ-1 clones used in this study were provided by T. Tanabe (Tokyo Medical and Dental University, Tokyo, Japan). Calcium channel currents were recorded 2–4 d after oocyte injection by standard two-electrode voltage clamp using a Warner amplifier (OC-725B) at 20–22°C, and data were collected using pClamp6 software (Axon Instruments, Foster City, CA). Microelectrodes were filled with 3 M KCl, and the resistances of the current and voltage electrodes were 0.3–1.5 MΩ. Data were filtered at 2 kHz and sampled at 10 kHz. Currents were recorded in a chloride-free bath containing (in mM): 5 $Ba(OH)_2$, 5 HEPES, 85 TEA-OH, and 2 KOH, pH adjusted to 7.4 with methanesulfonic acid. In experiments with the peptide toxin ω-CTx-MVIIC (Peptide Institute Inc. Osaka, Japan), the 5 mM Ba^{2+} solution was supplemented with 0.1 mg/ml cytochrome *c* to saturate nonspecific peptide binding sites. Cytochrome *c* at 0.1 mg/ml had no noticeable effect on recorded Ba^{2+} currents. Peptides were reconstituted according to the manufacturer's instructions (100 μM stock solutions in sterile, deionized water). Fresh dilutions of the peptide were made immediately before use. Currents typically ranged between 0.8 and 2.5 μA, and leak currents were between 20 and 100 nA. Data were analyzed using pClamp6 software (Axon Instruments) and Excel 7.0 (Microsoft Corp., Redmond, WA). The leak and capacitive currents were subtracted on line using a standard P/4 protocol. Curve fitting was performed with SigmaPlot version 5.0 (SSPS Inc., Chicago, IL).

Slow inactivation. Oocytes were held at −80 mV for ~2 min before a 300 msec reference pulse (I_R) to 0 mV (β_{4b}) or +10 mV (β_{4a}). After I_R, the membrane potential was stepped immediately to a conditioning pulse potential ranging from −100 mV to −20 mV (20 mV increments) and held for 5 min. During the conditioning pulse, a 300 msec test pulse (I_T) to 0 mV (β_{4b}) or +10 mV (β_{4a}) was applied every 15 sec. Data were normalized as the ratio of the maximum current at time T (I_T) divided by the maximum reference current (I_R). Data were fit to the double-exponential equation $I_T/I_R = A_1e^{-x/\tau 1} + A_2e^{-x/\tau 2}$, where I_T equals current at time T, I_R equals maximum reference current, x equals time in seconds, and A_1 and A_2 are components for the time constants τ_1 and τ_2, respectively. The SEM is shown for each data point unless the values are smaller than the symbol.

Recovery from slow inactivation. Currents were stabilized at −80 mV or −100 mV for ~2 min before a 300 msec reference pulse (I_R) to 0 mV (β_{4b}) or +10 mV (β_{4a}). After a 100 msec step to either −80 mV or −100 mV, the oocytes were held at a conditioning pulse potential of −30 mV for 5 min. Immediately after the conditioning pulse, a 300 msec test pulse was applied (I_1), and then the holding potential was stepped back to either −80 mV or −100 mV and 300 msec test pulses (I_{2-12}) were applied at 15 sec intervals starting at time 0 for a total of 3 min. Data were normalized as the ratio of the maximum current at time T (I_T) divided by the maximum reference current (I_R). Data were fit to the single exponential equation $I_T/I_R = I_\infty + Ae^{-x/\tau}$, where I_T equals current at time point T, I_R equals maximum reference current, I_∞ equals current remaining at end of protocol, x equals time in seconds, and A is the component for the time constant τ.

Voltage dependence of activation and inactivation. Voltage dependency of activation data was generated from *I–V* curves. Maximal currents were obtained from 300 msec depolarizations from a holding potential of −80 mV to various test potentials (−40 to +10 mV in 5 mV increments). Each individual recording was then normalized, inverted, and fit to the Boltzmann equation $\%I_{Ba} = 1/[1 + \exp(-(V_{test} - V_{1/2})/k)]$, where V_{test} equals *I–V* test potential, V_{pre} equals prepulse potential, $V_{1/2}$ equals midpoint of activation or inactivation, and k equals slope factor. The fit curves, $V_{1/2}$, and k values were then averaged and plotted as a function of membrane voltage.

Voltage dependency of inactivation data was obtained from peak currents elicited by a 300 msec maximal current test depolarization after a 20 sec conditioning prepulse to voltages ranging from −80 to +20 mV. Each individual recording was then normalized and fit to the Boltzmann equation $\%I_{Ba} = 1/[1 + \exp([V_{pre} - V_{1/2}]/k)]$, where V_{test} equals *I–V* test potential, V_{pre} equals prepulse potential, $V_{1/2}$ equals midpoint of activation or inactivation, and k equals slope factor. The fit curves, $V_{1/2}$, and k values were then averaged and plotted as a function of prepulse potential.

Pharmacology. Oocytes were held at a potential of −80 mV with maximal currents elicited by 150 msec test pulses to 0 mV (β_{4b}) or +10 mV (β_{4a}) every 15 sec for a total of 10 min. During recordings, oocytes were perfused at a constant rate of ~0.5 ml/min. Average current sizes for β_{4a} and β_{4b} complexes were 1.9 ± 0.2 μA (4–5 d of incubation) and 2.3 ± 0.3 μA (2–3 d of incubation), respectively. The data were fit to the single-exponential equation $I_T/I_R = I_\infty + Ae^{-x/\tau}$, where I_T equals maximum current at time point T, I_R equals maximum current at time point 0, I_∞ equals residual current at end of protocol, x equals time in seconds, and A is the component for the time constant, τ. The averaged rate constants ($1/\tau$) for the four ω-CTx-MVIIC concentrations (0.2, 0.6, 2, and 6 μM) were plotted as a log function of their concentration and were fit well by the equation $(\tau)^{-1} = k_{on}[Tx] + k_{off}$.

Northern blot analysis. A commercially available human neuronal tissue Northern blot [Multiple Tissue Northern (MTN) Blot brain II; Clontech] was probed with a nonspecific β_4 subunit probe (β_4ΔN; nucleotides 215–1628 plus ~300 bp of 3′ untranslated). A ^{32}P-labeled β_4 subunit probe was made with a nick translation kit (Promega, Madison,

WI) using the $\beta_4\Delta$N mutant as the template. The $\beta_4\Delta$N mutant is missing the first coding 147 bp corresponding to the 49 aa N terminus of β_4 [clone from Helton and Horne (2002)]. The MTN blot was hybridized overnight at 42°C in hybridization buffer [5× SSC, 5% w/v blocking reagent (Roche), 0.1% *N*-lauroylsarcosine, 0.02% w/v SDS, 50% w/v formamide] plus 100 μg/ml herring sperm DNA (Promega). The probe concentration was 1 million counts/ml. The blot was washed with successive stringency washes (four washes, 15 min each at 37°C) ranging from 2× SSC/0.1% SDS to 0.1× SSC/0.1% SDS. The blot was then exposed to radiographic film for 12 hr at −80°C. One microgram of cRNA for both β_{4a} and β_{4b} was run out on a 1% denaturing formaldehyde gel along with a poly(A)-tailed cRNA mass ladder (RNA Molecular Weight Marker 1; Roche). The β_{4a} cRNA is longer than the β_{4b} cRNA because of the additional ~400 nt of 5′ untranslated sequence.

Molecular modeling. The sequences for rat postsynaptic density-95 (PSD-95) (DLG4_rat) and human β_4 (CACNB4) were obtained (accession numbers P31016 and U95020) from the Swiss-prot database. Amino acids 10–96 of β_{4b} were aligned to residues 303–390 of PSD-95 based on secondary structure prediction (nnPredict) and visual inspection. For β_{4a}, amino acids 50–96 of β_{4b} were aligned to residues 345–390 of PSD-95. Using default parameters, the program MODELLER 6 (Sali and Blundell, 1993) was used to produce 50 models each of β_{4b} and β_{4a} structure based on the solved structure of the third PSD-95/Discs large/zona occludens-1 (PDZ) domain of PSD-95 (1BEF). Five models each were chosen for additional analysis based on the molecular probability density function (PDF) output from MODELLER and stereochemical analysis obtained through Ramachandran output from PROCHECK-NMR (Laskowski et al., 1993). The interactions between different atom types within these models and Cα root mean square deviation (RMSD) comparisons between the models and 1BEF were characterized with ERRAT (Colovos and Yeates, 1993). The β_{4a} and β_{4b} models chosen for comparison had the fewest disallowed residues (Ramachandran), lowest molecular PDF and RMSD values, and highest percentage of residues in acceptable conformations based on ERRAT and PROCHECK-NMR analysis. Models were visualized with the program MOLMOL (Koradi et al., 1996).

RESULTS

Alternative splicing of the β_4 subunit affects slow inactivation of $Ca_v2.1$ Ca^{2+} channels

In a previous study (Helton and Horne, 2002), we showed that $Ca_v2.1$ complexes containing the longer form of an alternatively spliced β_4 subunit N terminus, β_{4b} (49 aa), inactivated at more negative potentials in response to 20 sec conditioning prepulses than complexes containing a shorter form, β_{4a} (15 aa). To determine whether this response extended to slower types of inactivation, we examined in the present study the effects of β_{4a} and β_{4b} on $Ca_v2.1$ cumulative inactivation elicited by 5 min conditioning prepulses combined with stimulation at 0.25 Hz. Oocytes were stabilized at −80 mV before a 300 msec reference pulse (I_R) to potentials that were predetermined to give peak inward currents (β_{4b}, 0 mV; β_{4a}, +10 mV). The membrane potential was then stepped to and held at the conditioning prepulse potential (ranging from −100 to −20 mV) for 5 min. A 300 msec test pulse (I_T) was elicited from the conditioning prepulse potential every 15 sec (I_5 equals test pulse at 5 min). The kinetics of entry to slow inactivation for $Ca_v2.1$ complexes containing either β_{4a} or β_{4b} at −40 mV is shown in Figure 1*A*. For comparison purposes, we fit the data points for both β_{4a} and β_{4b} to two exponentials (smooth curves in the figure). The time constants for the fast component of entry (τ_1) for β_{4a} and β_{4b} were 28.6 ± 2.6 and 18.9 ± 1.2 sec, respectively, and the time constants for the slow component of entry (τ_2) were 769 ± 23.6 and 384 ± 14.8 sec, respectively. Overall, the I_T/I_R ratio for $Ca_v2.1$ complexes containing β_{4b} decreased to 0.5 in ~70 sec, whereas those containing β_{4a} required ~380 sec (data not shown). This indicated that β_{4b} caused a more than fivefold acceleration of the kinetics of slow inactivation. Representative current traces for reference and 5 min test pulses from a conditioning potential of −40 mV for $Ca_v2.1$ complexes containing β_{4a} (*top*) and β_{4b} (*bottom*) are shown in Figure 1*B*. As seen in the figure and as described in our previous study, $Ca_v2.1$ complexes containing β_{4a} underwent open-state fast inactivation faster than did complexes containing β_{4b}. After 5 min at −40 mV, the rate of fast inactivation was unaltered for complexes containing β_{4a}, and slowed only somewhat for complexes containing β_{4b}. The absence of any appreciable tail-current indicated that deactivation was not affected by prolonged depolarization. The I_5/I_R ratio is plotted against the range of conditioning potentials (−100 to −20 mV) in Figure 1*C*. The figure illustrates that the voltage dependence of $Ca_v2.1$ slow inactivation is shifted to the left for complexes containing β_{4b} relative to those containing β_{4a}. Half-maximal inactivation occurred at approximately

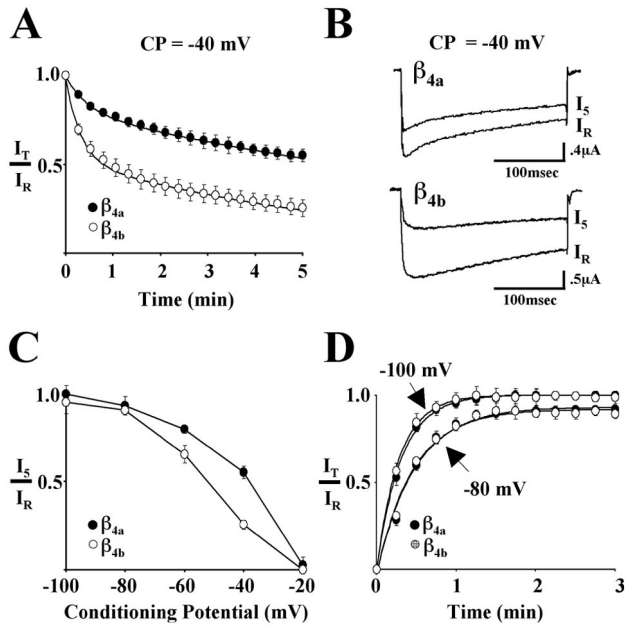

Figure 1. Effects of β_{4a} and β_{4b} on slow inactivation and recovery from slow inactivation of $Ca_v2.1$ Ca^{2+} channels. Studies were performed with *Xenopus* oocytes expressing α_{1A}, α_2/δ-1, and either β_{4a} or β_{4b}. Reference (I_R) and test current (I_T) traces were generated by 300 msec step depolarizations from various holding potentials to either 0 mV (β_{4b}) or +10 mV (β_{4a}). Maximum values from 300 msec I_R and I_T current traces were used to calculate I_T/I_R where indicated. Barium (5 mM) was used as the charge carrier. *A*, Influence of β_{4a} and β_{4b} on the development of slow inactivation at a conditioning potential (*CP*) of −40 mV. After a reference pulse (I_R) measured from a holding potential of −80 mV, oocytes were held at −40 mV for 5 min. During this time, 300 msec test pulses (I_T) were applied every 15 sec. Each *point* represents the mean value of I_T/I_R from 11 (β_{4a}) or 10 (β_{4b}) different recordings. The SEM is shown for each *point* unless the values were smaller than the *symbol*. The *solid lines* represent double-exponential fits to the data. *B*, Representative reference (I_R) and 5 min (I_5) current traces from $Ca_v2.1$ complexes containing either β_{4a} (*top*) or β_{4b} (*bottom*) generated as described in *A*. *C*, Voltage dependence of slow inactivation. The ratio of I_5 to I_R, generated as in *A*, plotted as a function of conditioning potential for $Ca_v2.1$ complexes containing either β_{4a} or β_{4b}. *Data points* represent the means of at least six determinations at a given membrane potential. *Lines* serve only to connect the *data points*. *D*, Influence of β_{4a} and β_{4b} on the time course of recovery from slow inactivation. After a 300 msec reference pulse (I_R) measured from a holding potential of either −80 or −100 mV, oocytes were held at −30 mV for 5 min. The membrane potential was then returned to either −80 or −100 mV, and sequential test pulses (I_T) were applied at 15 sec intervals for a total of 3 min. Each *point* represents the mean of at least seven different recordings. *Solid lines* represent the single-exponential fits of the data.

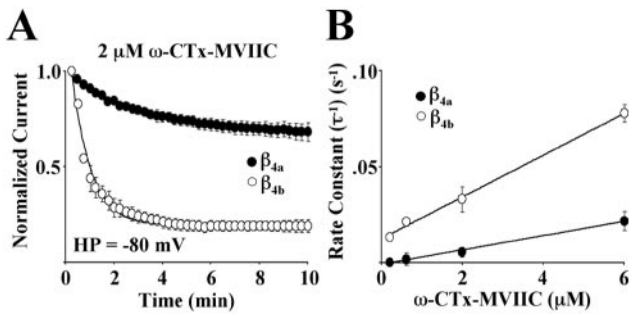

Figure 2. Effects of β_{4a} and β_{4b} on the blockade of $Ca_v2.1$ channels by ω-CTx-MVIIC. Studies were performed with *Xenopus* oocytes expressing α_{1A}, α_2/δ-1, and either β_{4a} or β_{4b}. *A*, Onset and degree of block by a 10 min exposure to 2 μM ω-CTx-MVIIC for $Ca_v2.1$ subunit combinations at a holding potential (*HP*) of −80 mV. Each *point* represents the mean of seven (β_{4a}) or eight (β_{4b}) different recordings. The SEM is shown for each *data point* unless smaller than the *symbol*. Onset of block for both subunit combinations was fit (*line*) to a single-exponential time course plus a constant. *B*, The rate constants for the time course of the onset of toxin block were determined from steady-state degree of block from single exponential fits at four different toxin concentrations (0.2, 0.6, 2, and 6 μM) for $Ca_v2.1$ complexes containing either β_{4a} or β_{4b}. The averaged rate constants were plotted as a function of toxin concentration (minimum of $n = 7$, ±SEM). The *line* represents a linear fit to the data.

−50 mV for complexes containing β_{4b} and −35 mV for β_{4a}. These values are ~10 mV (β_{4b}) and 5 mV (β_{4a}) more negative than were determined for inactivation in response to 20 sec conditioning prepulses (Helton and Horne, 2002). Figure 1*D* shows that recovery from 5 min of slow inactivation at −30 mV is nearly complete when the membrane potential is stepped back to −80 mV, and that there is no difference in the time course of recovery for $Ca_v2.1$ complexes containing either β_{4a} or β_{4b}. Recovery was somewhat faster and more complete when the membrane potential was stepped back to −100 mV. The recovery data at both potentials fit well to single exponentials. The time constants for recovery for β_{4a} and β_{4b} at −80 mV were 28.6 ± 2.0 and 27.8 ± 1.6 sec, respectively, and at −100 mV, 18.9 ± 0.5 and 17.2 ± 0.4 sec, respectively.

Alternative splicing of the β_4 subunit affects ω-CTx-MVIIC block of $Ca_v2.1$ Ca^{2+} channels

The results to this point indicate that changes in the structure of the β_4 subunit N terminus impact α_{1A} subunit structures that are important for many aspects of gating, including activation, open-state inactivation, and fast and slow closed-state inactivation. Given that recent evidence indicates that cytosolic determinants of two-membrane-spanning K^+ channel gating are coupled to changes in outer vestibule structure (Perozo et al., 1999; Jiang et al., 2002a,b), we next sought to determine whether alternative splicing of the β_4 subunit would affect the block of $Ca_v2.1$ channels by a marine snail peptide conotoxin, ω-CTx-MVIIC. Conotoxin interactions with voltage-gated Ca^{2+} channels are entirely extracellular and occur through binding sites located near H5 (P) helices in several of the six helix transmembrane-spanning motifs (Ellinor et al., 1994). Figure 2*A* shows the effects of 2 μM ω-CTx-MVIIC on $Ca_v2.1$ Ca^{2+} channel complexes expressed in *Xenopus* oocytes in the presence of either β_{4a} or β_{4b}. The oocytes were held at −80 mV for 10 min and stimulated every 15 sec. Under these conditions, ω-CTx-MVIIC associated with $Ca_v2.1$ complexes containing β_{4b} at a faster rate ($\tau = 50 \pm 0.75$ sec) than complexes containing β_{4a} ($\tau = 200 \pm 16$ sec). The loss of Ca^{2+} current resulting from slow inactivation over 10 min at −80 mV (<15%) was subtracted from the data plotted in the figure. Figure 2*B* demonstrates that as expected for a first-order reaction, the rate constants (τ^{-1}) for toxin block were linearly dependent on toxin concentration as described by the equation $(\tau)^{-1} = k_{on}$ [Tx] + k_{off}. Slopes of linear fits to the data for $Ca_v2.1$ complexes containing either β_{4a} and β_{4b} were 3.7×10^{-6} M^{-1} · sec^{-1} and 1.1×10^{-5} M^{-1} · sec^{-1}, respectively. This indicated that the on-rate (k_{on}) for toxin block was approximately threefold faster for $Ca_v2.1$ complexes containing β_{4b} than for those containing β_{4a}.

The molecular determinants of alternatively spliced β_4 subunit differential effects on gating and pharmacology are located within amino acids 10–20 of β_{4b}

Having characterized many of the functional consequences of alternative splicing of the β_4 A domain, we focused next on identifying the key structural determinants underlying the observed differences in effects. It was of particular interest to determine whether or not the effects of alternative splicing on gating and pharmacology could be assigned to separate structural entities. To accomplish this, we first created a series of β_{4b} deletion mutants in which the N terminus was shortened by multiples of 10 aa (β_{4b} Δ1–10 through β_{4b} Δ1–49) and characterized their effects on gating and pharmacology of $Ca_v2.1$ complexes. Figure 3*A–D* shows that, relative to full-length β_{4b}, deletion of the first 10 aa (β_{4b} Δ1–10) had no effect on the voltage dependence of activation (Fig. 3*A*), isochronal (20 sec prepulse) inactivation (Fig. 3*B*), onset into slow inactivation (Fig. 3*C*), or susceptibility to block by 2 μM ω-CTx-MVIIC (Fig. 3*D*). However, when amino acids 1–20 were removed (β_{4b} Δ1–20), both the voltage dependence of activation (Fig. 3*A*) and inactivation (Fig. 3*B*) of $Ca_v2.1$ complexes shifted to more depolarized potentials. As shown in the figure, the acquired gating properties were essentially identical those for $Ca_v2.1$ complexes containing β_{4a}. $Ca_v2.1$ complexes containing β_{4b} Δ1–20 also had a slower onset into slow inactivation (Fig. 3*C*) and were less susceptible to block by 2 μM ω-CTx-MVIIC (Fig. 3*D*). The effects of constructs β_{4b} Δ1–30, β_{4b} Δ1–40, and β_{4b} Δ1–49 were identical to those of β_{4b} Δ1–20 (data not shown). As a first attempt at determining whether the effects of β_{4b} Δ1–20 were simply the result of a decreased size of the β_{4b} N terminus, we reintroduced amino acids 1–10 to the N terminus of β_{4b} Δ1–20 to create the construct β_{4b} Δ10–20. As shown in Figure 3*A,B*, this did not restore the $V_{1/2}$ of either activation or inactivation to the hyperpolarized potentials characteristic of $Ca_v2.1$ complexes containing β_{4b}. Together, these results indicated that the molecular determinants responsible for the observed differences between $Ca_v2.1$ complexes containing β_{4a} versus β_{4b} were located in amino acids 10–20 of β_{4b}. Moreover, it was apparent that their influence extended to changes in both gating and pharmacology.

The β_4 A domain is a distant homolog of the third PDZ domain of PSD-95

With the results of the deletion experiments highlighting a specific location for the molecular determinants of β_{4b} gating and pharmacology effects, and with the observation that the β_{1b} A domain resembles PDZ domains (Hanlon et al., 1999), we began a systematic comparison of the β_{4b} sequence with similar regions of a number of PDZ domains. Unexpectedly, we found that the entire β_{4b} A domain was weakly homologous to the third PDZ domain of PSD-95 (Fig. 4*A*). Of the 87 aa that have been shown by x-ray crystallography to form the modular PDZ structure of PSD-95 (Doyle et al., 1996), 27 of these (~31%) are conserved in

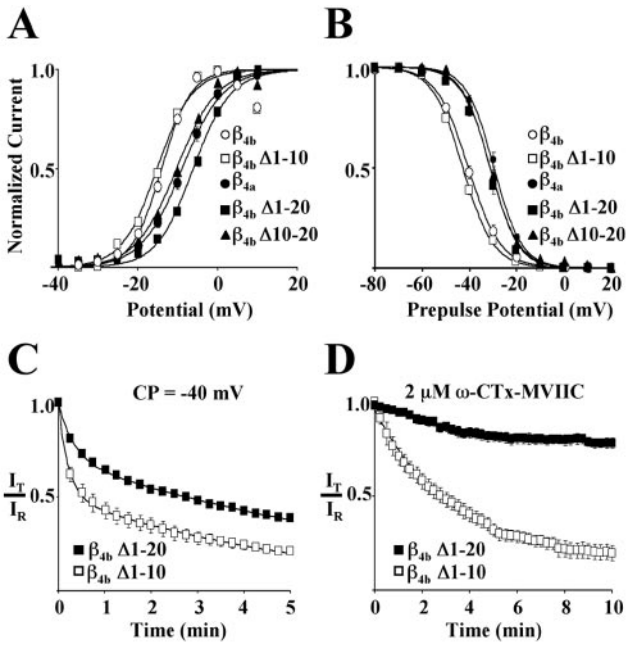

Figure 3. Localization of differential effects on $Ca_v2.1$ gating and pharmacology to β_{4b} N-terminal amino acids 10–20. The first 10 (β_{4b} Δ1–10), first 20 (β_{4b} Δ1–20), or second 10 (β_{4b} Δ10–20) aa of the N terminus of the β_{4b} subunit were removed using PCR. The deletion mutants as well as β_{4a} or β_{4b} were expressed with α_{1A} and $\alpha_2\delta$-1 in *Xenopus* oocytes. *A*, Effects of the N-terminal deletion mutants on the voltage dependency of activation of $Ca_v2.1$ channels. Plots were derived from averaged *I–V* data up to +10 mV for each β_4 subunit combination. *Data points* represent the means of the normalized data at a given membrane potential for a minimum of nine different recordings. *Smooth lines* represent single Boltzmann fits to the averaged data. *B*, Normalized, averaged isochronal inactivation curves for $Ca_v2.1$ complexes containing the various β_4 subunits. *Points* represent the means of the normalized data at a given membrane potential for a minimum of nine different recordings. *Smooth lines* represent single Boltzmann fits to the averaged data. *C*, Effects of β_4 N-terminal deletion mutants on the development of slow inactivation at a conditioning potential (*CP*) of −40 mV. Reference (I_R) and test (I_T) currents were generated as in Figure 1*A*. Each *point* represents the mean value of I_T/I_R from 13 (β_{4b} Δ1–10) or nine (β_{4b} Δ1–20) different recordings. The *solid lines* represent double-exponential fits to the data. *D*, Onset and degree of block by a 10 min exposure to 2 μM ω-CTx-MVIIC for $Ca_v2.1$ complexes containing β_{4b} Δ1–10 or β_{4b} Δ1–20. Data were generated as in Figure 2*A*. Each *point* represents the average of a minimum of seven recordings. The *solid lines* represent single-exponential fits to the data.

the β_{4b} sequence. Most importantly, these identities are conserved within key secondary structural elements, such as β-strand C and α-helix 2 of PSD-95. Also of note is the conservation of an RG(S/T)T motif in what would be the equivalent of the carboxylate binding loop (CBL) between β-strands A and B of PSD-95 and the loss of the GLGF motif that is extremely common among PDZ domain subtypes (Bezprozvanny and Maximov, 2001; Harris and Lim, 2001). Four of β_{4b} amino acids 10–20 (G10, D13, P15, and P18) were found in PSD-95. We used these as a starting point for further defining key β_{4b} residues involved in setting $Ca_v2.1$ gating parameters.

Figure 4*B* lists a series of site-directed mutants (*left*), along with their effects on the voltage dependence ($V_{1/2}$) of activation (*middle*) and inactivation (*right*) of $Ca_v2.1$ complexes. The $V_{1/2}$ values for complexes containing β_{4a} and β_{4b} are included for comparison. Interestingly, the first site-directed β_{4b} mutant tested, G10A, D13A, P15A, P18A, in which all four of the amino acids in common with PSD-95 were altered, displayed activation and inactivation properties similar to that of β_{4a}. To determine whether this was a specific effect, we altered four different amino acids in the β_{4b} 10–20 sequence to create the mutant, T11A, S17A, T19A, S20A. As shown in Figure 4*B*, $Ca_v2.1$ gating properties changed little in response to these mutations. $Ca_v2.1$ complexes containing the G10A, D13A, P15A, P18A mutant also had β_{4a}-like slow inactivation and pharmacological properties (data not shown). This indicates that the conserved amino acids are playing a defining role in the gating motif. To delineate the structure in more detail, we subsequently characterized six of the possible G10, D13, P15, P18 amino acid pairs for their effects on gating. Surprisingly, none of the pairs were absolutely essential for maintaining wild-type β_{4b} gating behavior, although small but statistically significant hyperpolarizing effects on activation were noted for five of the six pairs. To complete the alanine substitution study, we created the mutant H16A, which had a small but statistically significant effect on inactivation but not activation.

One interpretation of these results is that β_{4b} amino acids 10–20 form a ligand motif that interacts with a binding pocket located somewhere either on the α_{1A} subunit or on the β_4 subunit itself. The affinity of the ligand motif for its receptor site could be defined, for example, by the sum of the interactions of amino acids G10, D13, P15, and P18 with their individual targets. Any given pair may be capable of maintaining a binding interaction under the conditions of our experiments. As a first step toward addressing this possibility, we created three-dimensional structural models of the β_{4a} and β_{4b} A domains (Fig. 5*A,B*) using the real-space optimization method used in the computer program MODELLER (Sali and Blundell, 1993). The models were initiated using the distance and dihedral angle restraints derived from alignments with portions of the sequence of the third PDZ domain of PSD-95. For β_{4b}, amino acids 10–96 were aligned with amino acids 303–390 of PSD-95. There is 31% sequence identity over this region, which is considered minimally acceptable for this type of comparative modeling (Martí-Renom et al., 2000). For β_{4a}, amino acids 10–49 of β_{4b} were deleted from the alignment. Thus, the models do not include the first 15 aa of β_{4a} and the first 9 aa of β_{4b}. Figure 5*A* (*left*) shows that β_{4a} models as a compact structure containing three β-sheets and 2 α-helices. Stereochemical quality assessment of the model using PROCHECK-NMR (Laskowski et al., 1993) identified 41 residues (87.7%) in most favored regions, 5 (10.6%) in additional and generously allowed regions, and 1 (2.1%) in a disallowed region. Calculation of the electrostatic surface potential using MOLMOL (Koradi et al., 1996) reveals that the face of the molecule as oriented in Figure 5*A*, *left,* contains a pocket of negative charge (red residues) between the two α-helices (Fig. 5*A*, *right*). Figure 5*B*, *right* and *left*, illustrates that the overall effect of alternative splicing to form β_{4b} is to bury the charged pocket beneath three additional β-sheets. Interestingly, the molecule acquires as the result of splicing a positively charged binding pocket (blue residues) in what would be the equivalent of the CBL in PSD-95 (Fig. 4*A*). The stereochemical quality of the β_{4b} model as shown is not quite as good as that for β_{4a}. PROCHECK-NMR identified 64 residues (79%) in most favored regions, 11 residues (13.6%) in additional allowed regions, and 3 residues (3.7%) each in generously allowed and disallowed regions. Two of the three disallowed residues (R30 and K34) flank what would be the equivalent PSD-95 β-sheet B. Together with the loss of the highly conserved PDZ GLGF sequence, these results are consistent with the notion that through evolution this region of the β_{4b} structure has evolved

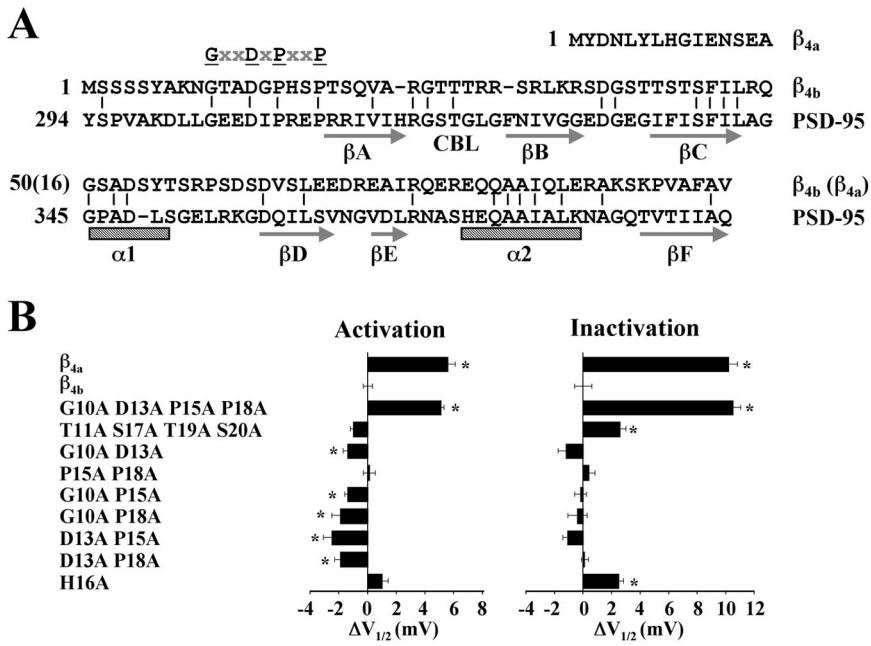

Figure 4. The β_4 subunit is a distant homolog of PSD-95. Identification of a conserved GXXDXPXXP motif critical to $Ca_v2.1$ gating. *A*, Amino acid alignment of the A domains of the human spinal cord β_{4a} (amino acids 1–63) and β_{4b} (amino acids 1–97) subunits with the third PDZ domain (amino acids 294–391) of PSD-95. *Vertical bars* denote identical amino acids between β_{4b} and PSD-95. Important amino acids involved in modulating the leftward shift in the voltage dependence of activation and inactivation of β_{4b} (GXXDXPXXP) are highlighted. *Arrows* and *hatched bars* represent predicted α-helices and β-strands of the third PDZ domain of PSD-95, respectively. *B*, Differences in the $V_{1/2}$ values of activation and inactivation of β_{4a}, β_{4b}, and β_{4b} N-terminal amino acid mutants. *Solid bars* represent average $V_{1/2}$ values of a minimum of nine different recordings for each β_4 subunit variant. Positive or negative shifts in the $V_{1/2}$ values (in millivolts) of activation and inactivation of β_{4a} and β_{4b} mutants are relative to the $V_{1/2}$ values of activation and inactivation of β_{4b}. Currents were generated as described in Figure 3, *A* and *B*. The SEM for each bar is shown. *Asterisks* denote statistical significance ($p < 0.05$) by a Student's two-sample equal variance *t* test.

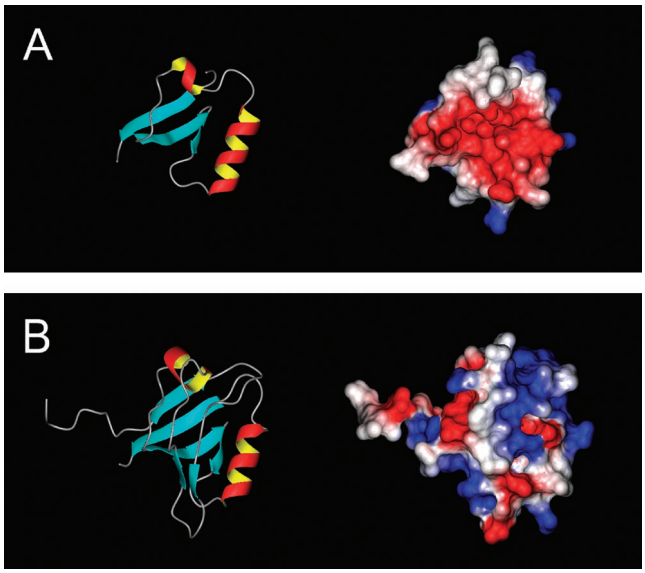

Figure 5. Real-space optimization structural models of the A domains of β_{4a} (*A*) and β_{4b} (*B*) based on sequence identities with the third PDZ domain of PSD-95. Ribbon (*left*) and electrostatic surface potential (*right*) diagrams were created using MOLMOL (Koradi et al., 1996). For ribbon diagrams, *arrows* indicate β-strands, and *helices* indicate α-helices. For surface potential diagrams, *red*, *white*, and *blue* regions indicate negatively charged, hydrophobic, and positively charged amino acids, respectively.

away from the capacity to bind C-terminal peptide motifs. Of most importance to our present results, however, is the observation that β_{4b} amino acids 10–20 model as an extended arm (pointing to the *left* in Fig. 5*B*, *right, left*) that may serve as a ligand motif. Interestingly, the orientation of the arm appears to be dictated by the isomerization state of proline18 (data not shown).

Differential distribution of alternatively spliced β_4 subunit mRNA

We noted in our previous study (Helton and Horne, 2002) that, based on extensive cDNA library screening, β_{4a} was the predominant alternatively spliced variant of the β_4 subunit expressed in human spinal cord. To confirm this observation, we performed a comparative Northern blot analysis using a commercially available multiple tissue Northern blot (Human Brain II; Clontech) and a β_4 cDNA probe containing sequence common to both β_{4a} and β_{4b}. The mRNAs for β_{4a} and β_{4b} can be readily distinguished by their distinct migration pattern in agarose-formaldehyde gels (Fig. 6*A*). The results of the Northern blot analysis, shown in Figure 6*B*, were striking, revealing that not only was β_{4a} the predominant form of β_4 subunit in the spinal cord, but also in other "reptilian" portions of the human CNS such as the medulla and putamen. Moreover, β_{4a} was the predominant form of β_4 subunit expressed in evolutionarily older regions of the cerebrum, the temporal lobe, and occipital pole. In marked contrast, β_{4b} was highly expressed in the most recent and most highly integrative region of the cerebrum, the frontal lobe. The two forms of the β_4 subunit were equally expressed in the cerebellum.

A basic local alignment search tool search of the human genome (Altschul et al., 1990) with β_4 sequences revealed that the exons coding for alternatively spliced forms of the β_4 subunit A domain are distributed widely on human chromosome 2. Figure 6*C* shows that, depending on the splice variant, the coding sequence for the β_4 PDZ domain is contained within three (β_{4a}) or four (β_{4b}) exons spread out over ~218,000 bases. The coding sequence for the GXXDXPXXP motif is included in the 5′-most exon of a pair of short exons that code for β_{4b} amino acids 1–49. Assembly of the β_{4b} mRNA requires that three RNA segments (536 bases, 214,959 bases, and 2329 bases) be spliced out. The short exon coding for the first 15 aa of β_{4a} lies between the β_{4b} N-terminal exons and the exon coding amino acids 50–89 and 16–55 of β_{4b} and β_{4a}, respectively. By comparison, the third PDZ domain of PSD-95 is encoded by two exons separated by a 200 bp intron (data not shown).

DISCUSSION

We have identified an alternatively spliced proline-rich motif in the Ca^{2+} channel β_4 subunit that has considerable influence over gating of neuronal $Ca_v2.1$ Ca^{2+} channels. Given that the motif also affects extracellular toxin binding, it is likely that the inter-

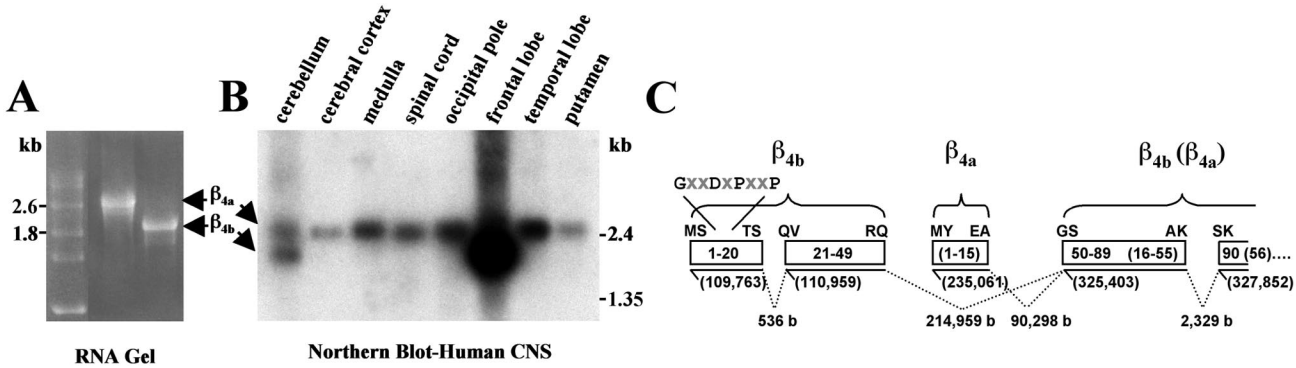

Figure 6. Differential distribution of β_{4a} and β_{4b} mRNA in the human CNS. *A*, Electrophoresis of full-length β_{4a} (*left*) and β_{4b} (*right*) cRNAs (includes 5′ and 3′ untranslated) in a 1% agarose formaldehyde denaturing gel. RNA markers (in kilobases) are indicated on the *left*. *B*, Northern blot analysis performed with human multiple tissue blot (Human Brain II; Clontech) and a ^{32}P-labeled β_4 subunit probe (coding nucleotides 215–1628 plus ~300 bp 3′ untranslated sequence). Molecular masses on the *right* correspond to labeled blot markers. *C*, A human β_4 subunit genome map depicting the lengths of intron sequences (b, bases) between alternatively spliced β_{4a} and β_{4b} N-terminal exons and the beginning of exon 2. *Solid lines* represent exons, and *dashed lines* represent introns. *Numbers* in *parentheses* below *solid lines* indicate position on chromosome 2. *Boxes* indicate protein sequence (β_{4a} in *parentheses*). The first and last two amino acids of each sequence are indicated above each *box*.

action of this motif with its binding site has wide-reaching impact on resting and open-state Ca^{2+} channel conformations. This notion is supported by recent images of the conformational changes that occur with gating of bacterial two-membrane-spanning K^+ channels (Liu et al., 2001; Jiang et al., 2002a,b). Like eukaryotic six-membrane-spanning K^+ channels, KcsA and MthK channels are tetramers that pack with fourfold symmetry around a central pore (Doyle et al., 1998; Jiang et al., 2002a). The principal structural elements of KcsA and MthK from N to C terminus include an outer transmembrane helix (M1), a pore helix (P), and an inner transmembrane helix (M2). These correspond to S5, H5, and S6 segments of voltage-gated Ca^{2+} channels, respectively. In the closed conformation of the KcsA structure, the four M2 helices are straight and arranged such that they form the walls of an inverted teepee that narrows from a 12 Å diameter at its center to a 4 Å pore at its tip (Doyle et al., 1998). After opening, the KcsA M2 helices tilt away from the permeation pathway and rotate about their helical axis (Liu et al., 2001). In MthK, bending and splaying of the inner helices after opening expands the diameter of the pore threefold (Jiang et al., 2002a,b). The nearly 30° bend occurs at a "gating hinge" corresponding to a glycine residue just below the selectivity filter. Applying a radial-outward force on the intracellular aspects of the inner helices places a torque on the gating hinge such that a conformational change is transmitted the full length of the M2 helix. This results in a widening of the outer vestibule [Jiang et al. (2002b), see supplementary information (movie)]. It is has been hypothesized that similar mechanical forces are at work in the gating of voltage-gated Ca^{2+} channels (Jiang et al., 2002b).

Considered in the context of this mechanical framework, our results suggest that an interaction of the β_{4b} ligand motif with an inner aspect of the $Ca_v2.1$ complex either directly or indirectly fine-tunes the torque experienced by α_{1A} S6 segments. In so doing, the interaction alters the conformation of the voltage sensor or gate (or both) as well as the outer vestibule. This would explain why alternative splicing of the β_4 subunit would affect both gating and toxin sensitivity. Given the potential for the ligand motif interaction to occur over a wide range (Helton and Horne, 2002), it is not possible from our results to pinpoint which S6 helices might be most affected. And although our ω-CTx-MVIIC binding results might be providing some direction, a previous study has shown that ω-CTx-GVIA binding to α_{1B} is affected by alterations in any of the four P loops that make up the outer vestibule (Ellinor et al., 1994). A case can be made for an indirect effect on the IS6 helix, because the primary α_1-β_4 subunit interaction occurs on the intracellular loop between homology domains I and II (I-II loop) (Pragnell et al., 1994). This is consistent with a previous study showing that IS6 is a critical determinant of voltage-dependent inactivation in $Ca_v2.1$ and $Ca_v2.3$ channels (Zhang et al., 1994). However, site-directed mutagenesis and domain-swapping studies have highlighted the equal importance of IIS6, IIIS6, and IVS6 in Ca^{2+} channel gating (for review, see Stotz and Zamponi, 2001; Shi and Soldatov, 2002), making the case for direct effects on these S6 helices equally plausible. It is interesting that many of the proteins that have evolved to modulate Ca^{2+} channel gating target α_1 I-II (β subunits, $G_{\beta\gamma}$ subunits, protein kinase C) and II-III loops (syntaxin, synaptotagmin, and synaptosomal-associated protein-25). The IS6 and IIS6 (but not IIIS6 or IVS6) helices of $Ca_v2.1$, 2.1, and 2.3 Ca^{2+} channels have glycines in hinge positions comparable with those present in KcsA and MthK (see alignments in Horne et al., 1993).

Despite extensive binding studies with β_4 subunits, there is currently no evidence to support the notion that the β_{4b} N terminus binds directly to α_{1A} subunits (Walker et al., 1998, 1999). One possible explanation for this is that the interaction is too weak to be detected in solution binding assays. The other possibility is that the α_{1A} subunit is not the primary binding target. The sequence of the ligand motif (GXXDXPXXP) may provide an important clue as to the nature of its own binding site. Proline-rich motifs are common within the primary structures of many ligands important for protein–protein interactions (for review, see Kay et al., 2000; Macias et al., 2002). Src homology 3 (SH3) and WW domains, for example, recognize proline-rich sequences containing a core PXXP, where X denotes any amino acid. These sequences adopt a PPII helix conformation that presents a hydrophobic surface as well as backbone carbonyls that are ideal for hydrogen bonding. Proline-rich ligands bind with low affinity, allowing for rapid modulation and added versatility in signaling pathways. In many respects, the β_{4b} ligand motif resembles the serine/threonine proline motifs recognized by group IV WW domains (Sudol and Hunter, 2000). As is the case for the β_{4b}

motif, the structural basis for recognition of these motifs is based on the summed contributions of a series of side-chain interactions, none of which is absolutely essential for ligand binding (Verdecia et al., 2000). It is possible that the β_{4b} proline-rich motif binds to its own B domain, which is structurally similar to SH3 and WW domains (Hanlon et al., 1999). This possibility is supported by what is known about related membrane-associated guanylate kinase family proteins in which intramolecular interactions are a key aspect of their functional diversity (Dimitratos et al., 1999).

To date, no specific function has been assigned to the GXXDXPXXP motif of the third PDZ domain of PSD-95. Most attention has been paid to the structure of the carboxylate binding loop to which it is immediately adjacent (Doyle et al., 1996) (Fig. 4, *CBL*). A partial list of the proteins that interact specifically with the third PDZ domain of PSD-95 include the cell-surface neuroligins (Irie et al., 1997), the microtubule binding protein cysteine-rich interactor of PDZ 3 (Niethammer et al., 1998), the Rho effector protein citron (Zhang et al., 1999), and the β_1 adrenergic receptor (Hu et al., 2000). It would be interesting to determine whether the GXXDXPXXP motif of PSD-95 plays a role maintaining the structure of the CBL. Such a role could also be considered for the GXXDXPXXP motif of β_{4b}. As is apparent in the β_{4b} A domain model structure (Figs. 4*A*, 5*B*), the sequences of β_{4b} corresponding to the hydrophobic CBL and β-strand B of PSD-95 are highly positively charged. It is possible, as is true for some PDZ domains (Cuppen et al., 1998), that this region binds to an internal (as opposed to a C-terminal) negatively charged domain. Interestingly, the immediate 5′ sequence of the II-III loop of $Ca_v2.1$ and $Ca_v2.2$ Ca^{2+} channels fits this description, because it is densely packed with glutamate residues. Moreover, several lines of evidence point to the II-III loop as a critical determinant of channel gating and pharmacology. Similar to the effects of β_{4b} on α_{1A}, binding of syntaxin to a "synprint site" just downstream from this region in the II-III loop of α_{1B} shifts the $V_{1/2}$ of inactivation to more hyperpolarized potentials (Bezprozvanny et al., 2000) and accelerates entry into slow inactivation (Degtiar et al., 2000), and an α_{1B} splice variant that lacks a large portion of the II-III linker region (Δ1) (Kaneko et al., 2002) inactivates at more depolarized potentials and is less sensitive to ω-CTx-MVIIA than is the full-length $Ca_v2.2$ variant.

Viewed from the perspective of changing Ca^{2+} channel function, the differential distribution of β_{4a} and β_{4b} subunit mRNA displayed in Figure 6*B* provides an unexpected snapshot of the evolution of forebrain synapses. It raises the possibility that with the introduction of β_{4b} to the genome, synapses acquired properties that fit better with the overall demand to organize complex neural networks. It could be that with the advent of $Ca_v2.1$ complexes that enter more readily into closed inactivation states (Fig. 1*A,C*) without perceptible gain in time required for recovery (Fig. 1*D*), synapses inherited an enhanced mechanism for synaptic plasticity. In this regard, short-term synaptic depression has been linked to Ca^{2+} channel inactivation (Forsythe et al., 1998) through mechanisms shown to be β subunit dependent (Patil et al., 1998). This form of short-term synaptic plasticity has been implicated in cortical gain control (Abbott et al., 1997) and low-pass temporal filtering (Fortune and Rose, 2001). In addition, long-lasting $Ca_v2.1$ channel inhibition has been identified as the mechanism underlying certain forms of long-term synaptic depression (Robbe et al., 2002). Accordingly, our future studies will be directed toward characterizing the responsiveness of Ca_v2 Ca^{2+} channels containing alternatively spliced β_4 subunits to changes in more dynamic regulatory inputs, such as neuronal firing frequency and action potential waveform.

REFERENCES

Abbott LF, Varela JA, Sen K, Nelson SB (1997) Synaptic depression and cortical gain control. Science 275:220–224.

Altschul SF, Gish W, Miller W, Myers EW, Lipman DJ (1990) Basic local alignment search tool. J Mol Biol 215:403–410.

Berjukow S, Marksteiner R, Sokolov S, Weiss RG, Margreiter E, Hering S (2001) Amino acids in segment IVS6 and β-subunit interaction support distinct conformational changes during $Ca_v2.1$ inactivation. J Biol Chem 276:17076–17082.

Berrou L, Bernatchez G, Parent L (2001) Molecular determinants of inactivation within the I-II linker of α_{1E} ($Ca_v2.3$) calcium channels. Biophys J 80:215–228.

Bezanilla F (2000) The voltage sensor in voltage-dependent ion channels. Physiol Rev 80:555–592.

Bezprozvanny I, Maximov A (2001) PDZ domains: more than just a glue. Proc Natl Acad Sci USA 98:787–789.

Bezprozvanny I, Zhong P, Scheller RH, Tsien RW (2000) Molecular determinants of the functional interaction between syntaxin and N-type Ca^{2+} channel gating. Proc Natl Acad Sci USA 97:13943–13948.

Catterall WA (2000) Structure and regulation of voltage-gated Ca^{2+} channels. Annu Rev Cell Dev Biol 16:521–555.

Cha A, Snyder GE, Selvin PR, Bezanilla F (1999) Atomic scale movement of the voltage-sensing region in a potassium channel measured via spectroscopy. Nature 402:809–813.

Colovos C, Yeates TO (1993) Verification of protein structures: patterns of nonbonded atomic interactions. Protein Sci 2:1511–1519.

Cuppen E, Gerrits H, Pepers B, Wieringa B, Hendriks W (1998) PDZ motifs in PTP-BL and RIL bind to internal protein segments in the LIM domain protein RIL. Mol Biol Cell 9:671–683.

Degtiar VE, Scheller RH, Tsien RW (2000) Syntaxin modulation of slow inactivation of N-type calcium channels. J Neurosci 20:4355–4367.

Dimitratos SD, Woods DF, Stathakis DG, Bryant PJ (1999) Signaling pathways are focused at specialized regions of the plasma membrane by scaffolding proteins of the MAGUK family. BioEssays 21:912–921.

Doyle DA, Lee A, Lewis J, Kim E, Sheng M, MacKinnon R (1996) Crystal structures of a complexed and peptide-free membrane protein-binding domain: molecular basis of peptide recognition by PDZ. Cell 85:1067–1076.

Doyle DA, Morais-Cabral J, Pfuetzner RA, Kuo A, Gulbis JM, Cohen SL, Chait BT, MacKinnon R (1998) The structure of the potassium channel: molecular basis of K^+ conduction and selectivity. Science 280:69–77.

Ellinor PT, Zhang JF, Horne WA, Tsien RW (1994) Structural determinants of the blockade of N-type calcium channels by a peptide neurotoxin. Nature 372:272–275.

Forsythe ID, Tsujimoto T, Barnes-Davies M, Cuttle MF, Takahashi T (1998) Inactivation of presynaptic calcium current contributes to synaptic depression at a fast central synapse. Neuron 20:797–807.

Fortune ES, Rose GJ (2001) Short-term synaptic plasticity as a temporal filter. Trends Neurosci 24:381–385.

Glauner KS, Mannuzzu LM, Gandhi CS, Isacoff EY (1999) Spectroscopic mapping of voltage sensor movement in the Shaker potassium channel. Nature 402:813–817.

Hanlon MR, Berrow NS, Dolphin AC, Wallace BA (1999) Modeling of a voltage-dependent Ca^{2+} channel β subunit as a basis for understanding its functional properties. FEBS Lett 445:366–370.

Hans M, Urrutia A, Deal C, Brust PF, Stauderman K, Ellis SB, Harpold MM, Johnson EC, Williams ME (1999) Structural elements in domain IV that influence biophysical and pharmacological properties of human α_{1A}-containing high-voltage-activated calcium channels. Biophys J 76:1384–1400.

Harris BZ, Lim WA (2001) Mechanism and role of PDZ domains in signaling complex assembly. J Cell Sci 114:3219–3231.

Helton TD, Horne WA (2002) Alternative splicing of the β_4 subunit has α_1 subunit subtype-specific effects on Ca^{2+} channel gating. J Neurosci 22:1573–1582.

Horn R (2000) A new twist in the saga of charge movement in voltage-dependent ion channels. Neuron 25:511–514.

Horne WA, Ellinor PT, Inman I, Zhou M, Tsien RW, Schwarz TL (1993) Molecular diversity of Ca^{2+} channel α_1 subunits from the marine ray *Discopyge ommata*. Proc Natl Acad Sci USA 90:3787–3791.

Hu LA, Tang Y, Miller WE, Cong M, Lau AG, Lefkowitz RJ, Hall RA (2000) β_1-adrenergic receptor association with PSD-95: inhibition of receptor internalization and facilitation of β_1-adrenergic receptor interaction with *N*-methyl-D-aspartate receptors. J Biol Chem 275:38659–38666.

Irie M, Hata Y, Takeuchi M, Ichtchenko K, Toyoda A, Hirao K, Takai Y, Rosahl TW, Sudhof TC (1997) Binding of neuroligins to PSD-95. Science 277:1511–1515.

Jiang Y, Lee A, Chen J, Cadene M, Chait BT, MacKinnon R (2002a)

Crystal structure and mechanism of a calcium-gated potassium channel. Nature 417:515–522.
Jiang Y, Lee A, Chen J, Cadene M, Chait BT, MacKinnon R (2002b) The open pore conformation of potassium channels. Nature 417:523–526.
Kaneko S, Cooper CB, Nishioka N, Yamasaki H, Suzuki A, Jarvis SE, Akaike A, Satoh M, Zamponi GW (2002) Identification and characterization of novel human Cav2.2 (a1B) calcium channel variants lacking the synaptic protein interaction site. J Neurosci 22:82–92.
Kay BK, Williamson MP, Sudol M (2000) The importance of being proline: the interaction of proline-rich motifs in signaling proteins with their cognate domains. FASEB J 14:231–241.
Koradi R, Billeter M, Wuthrich K (1996) MOLMOL: a program for display and analysis of macromolecular structures. J Mol Graph 14:51–55:29–32.
Kozak M (1991) An analysis of vertebrate mRNA sequences: intimations of translational control. J Cell Biol 115:887–903.
Laskowski RA, Moss DS, Thornton JM (1993) Main-chain bond lengths and bond angles in protein structures. J Mol Biol 231:1049–1067.
Lin Z, Haus S, Edgerton J, Lipscombe D (1997) Identification of functionally distinct isoforms of the N-type Ca^{2+} channel in rat sympathetic ganglia and brain. Neuron 18:153–166.
Liu YS, Sompornpisut P, Perozo E (2001) Structure of the KcsA channel intracellular gate in the open state. Nat Struct Biol 8:883–887.
Macias MJ, Wiesner S, Sudol M (2002) WW and SH3 domains, two different scaffolds to recognize proline-rich ligands. FEBS Lett 513:30–37.
Martí-Renom MA, Stuart AC, Fiser A, Sanchez R, Melo F, Sali A (2000) Comparative protein structure modeling of genes and genomes. Annu Rev Biophys Biomol Struct 29:291–325.
Niethammer M, Valtschanoff JG, Kapoor TM, Allison DW, Weinberg TM, Craig AM, Sheng M (1998) CRIPT, a novel postsynaptic protein that binds to the third PDZ domain of PSD-95/SAP90. Neuron 20:693–707.
Patil PG, Brody DL, Yue DT (1998) Preferential closed-state inactivation of neuronal calcium channels. Neuron 20:1027–1038.
Perozo E, Cortes DM, Cuello LG (1999) Structural rearrangements underlying K+-channel activation gating. Science 285:73–78.
Pragnell M, De Waard M, Mori Y, Tanabe T, Snutch TP, Campbell KP (1994) Calcium channel β-subunit binds to a conserved motif in the I-II cytoplasmic linker of the α_1-subunit. Nature 368:67–70.
Robbe D, Alonso G, Chaumont S, Bockaert J, Manzoni AJ (2002) Role of P/Q-Ca^{2+} channels in metabotropic glutamate receptor 2/3-dependent presynaptic long-term depression at nucleus accumbens synapses. J Neurosci 22:4346–4356.
Sali A, Blundell TL (1993) Comparative protein modelling by satisfaction of spatial restraints. J Mol Biol 234:779–815.
Shi C, Soldatov NM (2002) Molecular determinants of voltage-dependent slow inactivation of the Ca^{2+} channel. J Biol Chem 277:6813–6821.
Stotz SC, Zamponi GW (2001) Identification of inactivation determinants in the domain IIS6 region of high voltage-activated calcium channels. J Biol Chem 276:33001–33010.
Stotz SC, Hamid J, Spaetgens RL, Jarvis SE, Zamponi GW (2000) Fast inactivation of voltage-dependent calcium channels. A hinged-lid mechanism? J Biol Chem 275:24575–24582.
Sudol M, Hunter T (2000) New wrinkles for an old domain. Cell 103:1001–1004.
Verdecia MA, Bowman ME, Lu KP, Hunter T, Noel JP (2000) Structural basis for phosphoserine-proline recognition by group IV WW domains. Nat Struct Biol 7:639–643.
Walker D, Bichet D, Campbell KP, De Waard M (1998) A β4 isoform-specific interaction site in the carboxyl-terminal region of the voltage-dependent Ca^{2+} channel α_{1A} subunit. J Biol Chem 273:2361–2367.
Walker D, Bichet D, Geib S, Mori E, Cornet V, Snutch TP, Mori Y, De Waard M (1999) A new β subtype-specific interaction in α_{1A} subunit controls P/Q-type Ca^{2+} channel activation. J Biol Chem 274:12383–12390.
Zhang JF, Ellinor PT, Aldrich RW, Tsien RW (1994) Molecular determinants of voltage-dependent inactivation in calcium channels. Nature 372:97–100.
Zhang W, Vazquez L, Apperson M, Kennedy MB (1999) Citron binds to PSD-95 at glutamatergic synapses on inhibitory neurons in the hippocampus. J Neurosci 19:96–108.
Zhong H, Li B, Scheuer T, Catterall WA (2001) Control of gating mode by a single amino acid residue in transmembrane segment IS3 of the N-type Ca^{2+} channel. Proc Natl Acad Sci USA 98:4705–4709.